The design of hydrodynamically lubricated journal bearings against yield

M Ciavarella[1]*, **P Decuzzi**[2], **G Demelio**[2], **G Monno**[2] and **D A Hills**[3]
[1]Mechanical Engineering Department, University of Southampton, UK
[2]Dipartimento di Progettazione e Produzione Industriale, Politecnico di Bari, Italy
[3]Department of Engineering Science, University of Oxford, UK

Abstract: The stress field induced by the half-Sommerfeld pressure distribution in an infinitely elongated bearing is studied in detail. A complex potential formulation for the stress field is employed to solve the elasticity problem, with the intention to compute the required strength according to the classical von Mises criterion. Example contour plots of the yield parameter $(\sqrt{J_2})/p_m$ are given and the position and magnitude of the maximum normalized von Mises parameter are determined for a range of working conditions, analytically when they are on the surface, i.e. for eccentricity ratios $\varepsilon < 0.6$, and semi-analytically for the cases where they are located subsurface, i.e. $\varepsilon > 0.6$. Surprisingly simple results are obtained for eccentricity ratios lower than about 0.7, namely a maximum of the von Mises parameter proportional to the mean pressure, permitting a simple rule to be developed for the design of bearings against yielding: if the bearing works with eccentricity ratios smaller than 0.7, and the average pressure is smaller than $1.22k$, where k is the yield stress of the material in pure shear, then yielding is avoided.

When bearings are used in the range of very high eccentricity ratios, a more refined calculation is needed, taking into account the actual value of the maximum von Mises parameter and the paper provides design charts for this purpose.

Keywords: design, hydrodynamic lubrication, journal bearings, yield

NOTATION

p_m	specific pressure
R	bearing radius
R_s	journal radius
W	bearing load per unit length
ε	relative eccentricity
μ	viscosity of oil
ψ	radial relative clearance
ω	angular speed of the journal

1 INTRODUCTION

Journal bearings are commonly designed against frictional overheating, by preventing the product pV from exceeding a critical value, where p is the nominal bearing pressure and V the peripheral speed of the journal. However, heat dissipation is not the only relevant design consideration and, as today's bearings are subject to large applied loads, often because of space limitations, extreme operating pressures often arise, concentrated over small arcs. Under these conditions, the peak lubricant pressure may reach three times the value of the nominal (average) design specific pressure, during bearing service. As a consequence of these very high contact pressures, an examination of the design of the bearing shells against yielding may be advisable. There have been only a few previous attempts to solve this problem [**1**–**3**], and the intention here is to expand the range of results available significantly, by providing explicit formulae, in closed form, for the severity of the stress state induced. The principal idealization in the formulation is the use of a stress representation within an infinite body. In reality, a formulation for a thin annular ring representing the bearing shell ought to be used, and a surrounding medium of finite dimensions representing the housing. However, although the shell and housing are elastically dissimilar, this mismatch will not have a profound effect on the stress state. Further, although the outer dimensions of the housing will also have an influence, it will be relatively small, as the severest state of stress is found on the shell surface (or, in a few cases, slightly subsurface), and the influence of remote boundaries will be small. The greatest advantage of the approach is that,

The MS was received on 21 July 1998 and was accepted after revision for publication on 15 December 1998.
**Corresponding author: CNR-IRIS Computational Mechanics of Solids (COMES), Str. Crocifisso 2/B, 70125 Bari, Italy.* E-mail: M.Ciavarella@area.ba.cnr.it.

perhaps surprisingly for a problem where the applied pressure has such a complex form, a closed-form solution for the stress state is found, so that numerical methods are avoided, and this is of importance in design procedures.

2 FORMULATION

The journal bearing itself is idealized as an infinite elongated shaft, rotating in a lubricated cylindrical hole built in an infinite elastic medium, which simulates the bushing (Fig. 1). The classical half-Sommerfeld oil pressure distribution is employed, i.e.

$$p(\theta, \varepsilon) = p_m \frac{2(\varepsilon^2 - 1)}{\sqrt{[\pi^2 - \varepsilon^2(\pi^2 - 4)]}} \frac{\sin\theta(2 + \varepsilon\cos\theta)}{(1 + \varepsilon\cos\theta)^2}, \quad \theta \in [0, \pi] \tag{1}$$

The active bearing arc is confined to the region $\theta \in [0, \pi]$ (see Section 12 of reference [4]), as the customary assumption is made that the oil film fails in the tension region. Here, p_m is the specific pressure for an infinitely elongated bearing [$p_m = W/(2R)$], where W is the load per unit width of the bearing and R its nominal radius (shell radius). The load depends on the eccentricity ratio ε, which is related to the dimensionless clearance ψ, and is characterized by the 'attitude angle' β, which is the angle formed by the load and the x axis (see Section 12 of reference [4] and also Appendix 1 of this paper):

$$W = 6\frac{\mu\omega}{\psi^2}\frac{\varepsilon}{2 + \varepsilon^2}\frac{R_s}{1 - \varepsilon^2}\sqrt{[(\pi^2 - \varepsilon^2(\pi^2 - 4)]} \tag{2}$$

$$\tan\beta = \frac{\pi}{2}\frac{\sqrt{(1 - \varepsilon^2)}}{\varepsilon} \tag{3}$$

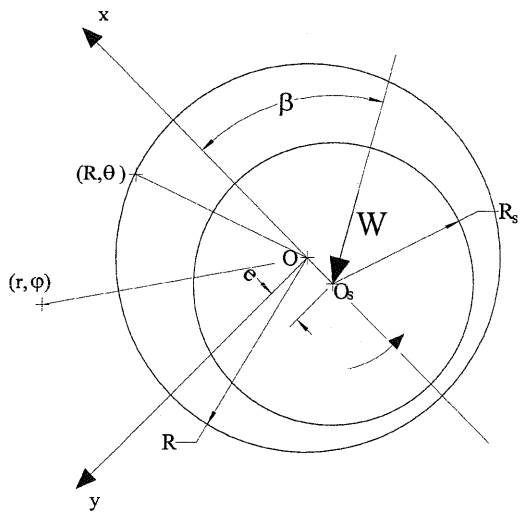

Fig. 1 Geometry of the journal bearing and symbols used

Here, ω is the angular speed of the shaft, R_s the journal radius, ψ the relative radial clearance [$\psi = (R - R_s)/R_s$] and ε the eccentricity ratio [$\varepsilon = e/(R - R_s)$]. The quantity e is the actual eccentricity.

In Fig. 2, the non-dimensional half-Sommerfeld pressure distribution around the bearing is shown as a function of the normalized angular position φ/π, for different eccentricity ratios in the range 0.1–0.9. The curves exhibit a peak whose magnitude and location change with eccentricity ratio. The application of a larger load results in an increase in ε, and this gives rise to a higher peak pressure. Its position also moves towards the end of the bearing active arc; the peak becomes sharper and develops a larger pressure localized over a small region of the shell. Note that, in the limit, as ε approaches unity, the pressure distribution tends to a radial line load, of infinite magnitude, applied at $\varphi = \pi$. However, long before this situation is reached the half-Sommerfeld pressure distribution itself loses validity.

Also, note from equation (2) that the relationship between the operating parameter ε and the applied load W is monotonic, i.e. a larger W implies a larger eccentricity ratio, as shown in Fig. 3, where the variation in the 'attitude angle' β with the eccentricity ratio ε is also illustrated.

2.1 Stress analysis

The bearing geometry is idealized as a shaft rotating in a lubricated cylindrical hole built in an infinite elastic and isotropic medium (Fig. 1). A complex potential formulation may conveniently be used, first to evaluate the internal stress field due to a line load applied on the surface of the hole of radius R, under transverse plane strain conditions. The internal stress field may be evaluated by employing the following relations, given by Green and Zerna [5] (see Section 8.18 of reference [5]):

$$\frac{\sigma_{rr}(z) + \sigma_{\phi\phi}(z)}{4} = \Omega'(z) + \overline{\Omega}'(\bar{z})$$

$$\frac{\sigma_{rr}(z) - \sigma_{\phi\phi}(z) + 2i\sigma_{r\phi}(z)}{4} = -\frac{R^2}{z\bar{z}}\Omega'\left(\frac{R^2}{\bar{z}}\right) - \frac{R^2}{z\bar{z}}\overline{\Omega}'(\bar{z}) + \left(\frac{R^2}{z} - \bar{z}\right)\overline{\Omega}''(\bar{z}) \tag{4}$$

where $z = r\,e^{i\varphi}$ is an arbitrary internal point, $\Omega(z)$ is an unknown complex potential depending on the boundary conditions. In particular, for a radial line load $F\,e^{i\theta}$, applied on the periphery of the hole (see Section 8.21 of reference [5]),

$$\Omega'(z) = \frac{F}{4\pi}\left[\frac{\kappa}{(\kappa + 1)z} - \frac{1}{z - z_0}\right]e^{i\theta} \tag{5}$$

where κ is Kolosoff's constant ($\kappa = 3 - 4\nu$, for plane strain problems). Subsequently, the complex relations (8) and (9)

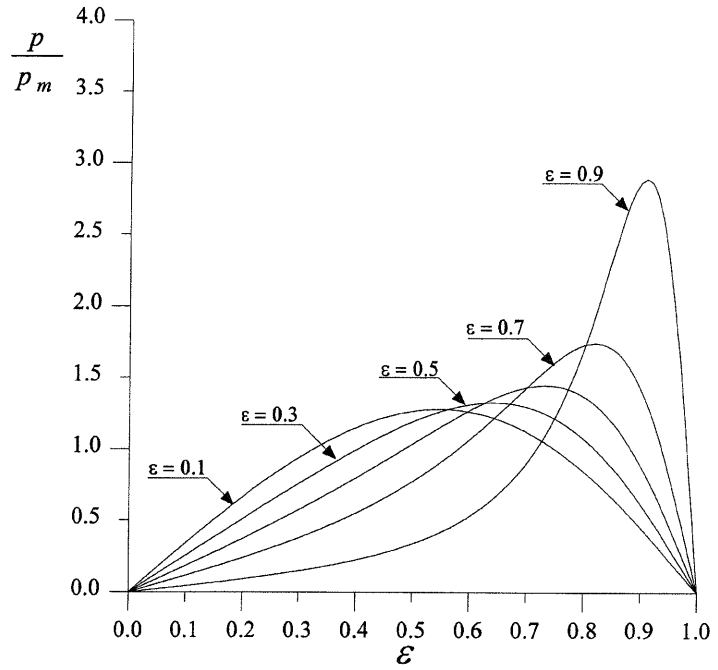

Fig. 2 The half-Sommerfeld normalized pressure distribution along the bearing active arc, for different eccentricity ratios ε

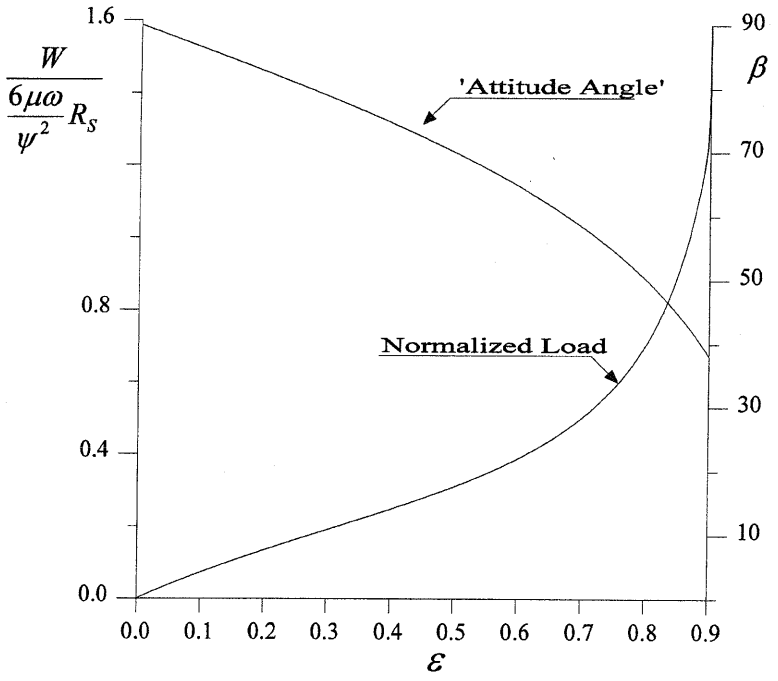

Fig. 3 The normalized applied load and the 'attitude angle' against the eccentricity ratio

will be written in a concise polar notation, with the axis set as shown in Fig. 1:

$$\sigma_{ij}(\rho, \varphi, \theta) = \frac{F}{\pi R} g_{ij}(\rho, \varphi, \theta), \qquad \{i, j\} = \{r, \varphi\} \tag{6}$$

where $\rho = r/R$ is the dimensionless radial abscissa and $g_{ij}(\rho, \varphi, \theta)$ are real influence stress functions, given explicitly in Appendix 2. For a continuous distribution of line loads, such as the case of oil pressure $p(\theta; \varepsilon)$ around the hole surface, the stress field takes the form

$$\sigma_{ij}(\rho, \varphi) = \frac{1}{\pi}\int_0^{2\pi} p(\theta; \varepsilon) g_{ij}(\rho, \varphi, \theta)\, \mathrm{d}\theta, \qquad \{i, j\} = \{r, \varphi\} \tag{7}$$

At this stage, traditional quadrature schemes may be employed to evaluate the previous integrals [**6**], but care must be taken when points are very close to the surface where singularities arise, because g_{ij} is singular for ρ equal to unity. However, stresses at the hole's surface ($\rho = 1$) may be evaluated analytically, as reported in reference [**1**]:

$$-\sigma_{rr}(\varphi) + \sigma_{\varphi\varphi}(\varphi) = \frac{1}{\pi}\int_0^{2\pi} p(\theta; \varepsilon)[g_{rr}(\varphi, \theta) + g_{\varphi\varphi}(\varphi, \theta)]\, \mathrm{d}\theta = \frac{1 - \varepsilon^2}{\sqrt{[\pi^2 - \varepsilon^2(\pi^2 - 4)]}} I(\varphi) \tag{8}$$

where

$$\sigma_{rr}(\varphi) = -p(\varphi), \qquad \sigma_{\varphi\varphi}(\varphi) = 0$$

$$I(\varphi) = \begin{cases} \dfrac{2\pi\kappa_1 \sin\varphi}{\sqrt{(1 - \varepsilon^2)}} + \dfrac{2(1 - 2\varepsilon\kappa_1 \cos\varphi)}{1 - \varepsilon^2} + \dfrac{1}{\varepsilon}\log\left(\dfrac{1 + \varepsilon}{1 - \varepsilon}\right), & \varepsilon > 0 \\ 2\pi\kappa_1 \sin\varphi + 4, & \varepsilon = 0 \end{cases} \tag{9}$$

with $\kappa_1 = \kappa/(\kappa + 1)$. Note that the stress analysis has been carried out under transverse plane strain conditions, consistent with the hypothesis of an infinite elongated bearing, and may be considered acceptable for length–diameter ratios of, say, $L/R \geqslant 3$.

3 RESULTS AND DISCUSSION

The main objective of studying the stress field induced in the journal bearing shells is to determine the location of points of first yield and to evaluate the magnitude of the normalized von Mises parameter $(\sqrt{J_2})/p_m$ (see Section 3.8 of reference [7]) at that point, so that the risk of the onset of plasticity can be estimated. The points of first yield were located by employing a numerical optimization routine.

Many contour plots of the dimensionless von Mises parameter have been produced for different eccentricity ratios ε, some of which are reproduced in Fig. 4. For small applied loads, the points of first yield are located at very small depths, which may be assumed to be on the surface. They also steadily track over the surface with increasing ε, following the peak pressure. This is summarized in Figs 4a to c, where the increasing skewness of the contours with increasing ε is also evident. Further, for sufficiently large eccentricity ratios ($\varepsilon \geqslant 0.6$), the severest state of stress sinks progressively beneath the surface; this was not recognized in reference [**1**], where only surface values of the von Mises parameter were considered. The point of first yield reaches then a maximum depth and then moves back closer to the surface, while still migrating towards the exit side of the bearing active arc, as ε is increased. Note that, for $\varepsilon = 1$, the point of first yield should be on the surface at $\varphi = \pi$, according to the half-Sommerfeld distribution, if this were a practically relevant case. It is worth noting that, as the applied load W is increased, the most heavily stressed area (where the von Mises parameter is greater than 90 per cent of the maximum value) becomes larger and moves towards the end of the contact arc, as summarized in Fig. 5. The locus of physical location of the maximum yield parameter $(\sqrt{J_2})/p_m$ is clearly represented in Fig. 6.

When the operating eccentricity ratios are small, the pressure distribution is almost flat in shape and the applied load W is distributed over all the active arc of the bearing, giving rise to a stress field of modest intensity. On the other hand, for large eccentricity ratios ($\varepsilon > 0.7$), the pressure distribution exhibits a sharp peak, and the bearing load is concentrated over a smaller area of the surface. Therefore, the stress field is more severe, although the fact that the absolute maximum may be submerged means that the plastic zone at loads only just exceeding the elastic limit are totally confined.

As expected intuitively, the magnitude of the dimensionless von Mises parameter increases monotonically with increasing eccentricity ratio (i.e. as the applied load becomes greater). This is clear in Fig. 7, where the maximum magnitude of $(\sqrt{J_2})/p_m$ is plotted against the eccentricity ratio. A comparison between subsurface and surface maxima is also shown. It is evident that, for $\varepsilon \leqslant 0.7$, the maximum von Mises parameter is almost constant, independently of the fact that, for $\varepsilon > 0.6$, it is located subsurface and equals $[(\sqrt{J_2})/p_m]_{max} \approx 0.82$.

By setting $\sqrt{J_2} = k$, where k is the yield stress of the material in pure shear, i.e. invoking the von Mises criterion and the definition of the specific pressure, the elastic limit of the problem may be found to be

$$p_m \leqslant 1.22k \qquad \text{for } \varepsilon \leqslant 0.7 \tag{10}$$

For cases where the bearing can satisfactorily operate with $\varepsilon \leqslant 0.7$, the design process is finished, as we need to check only that the pressure at the maximum operating ε is lower than $1.22k$. However, modern bearings are commonly

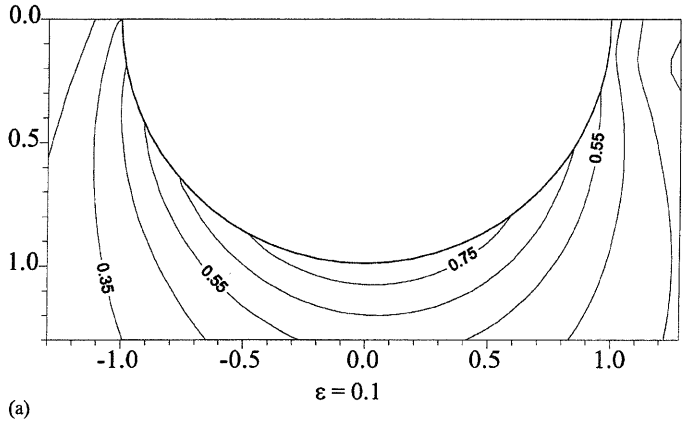

(a)

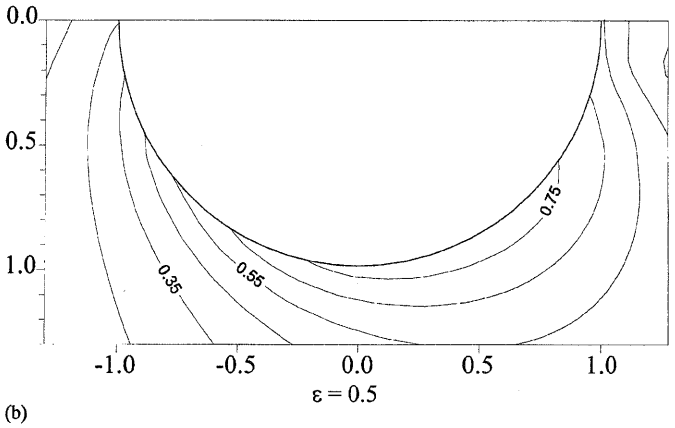

(b)

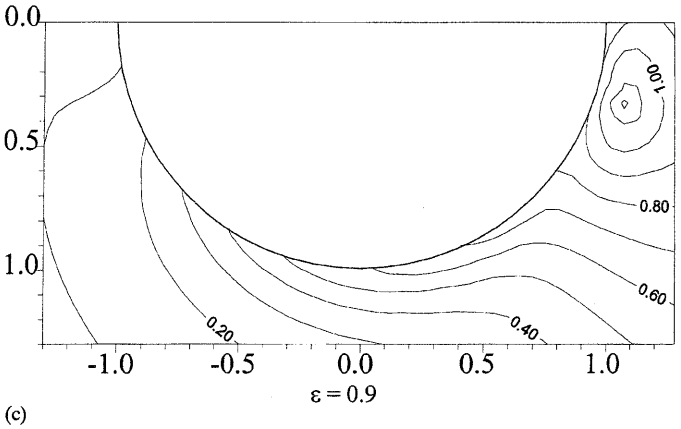

(c)

Fig. 4 The contours of the dimensionless von Mises parameter $\sqrt{J_2}/p_m$, under transverse plane strain ($\nu = 0.3$)

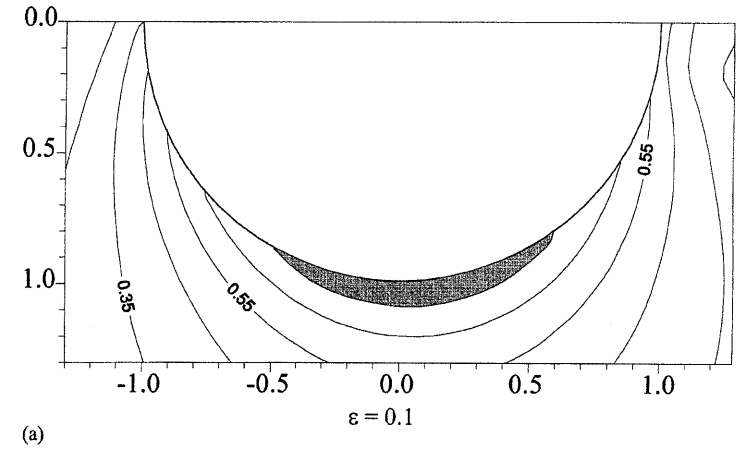

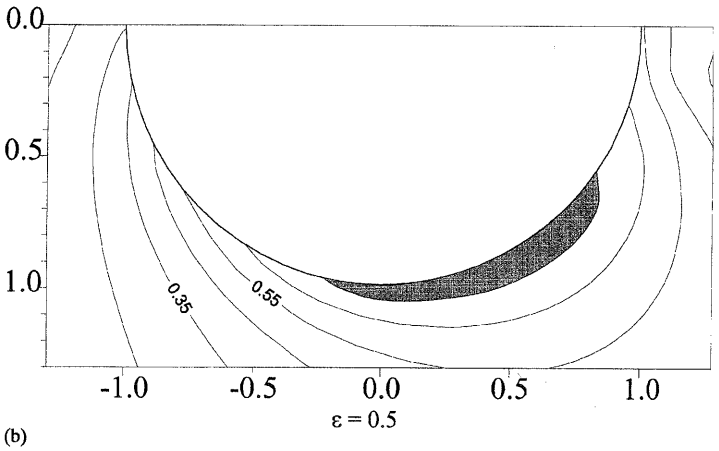

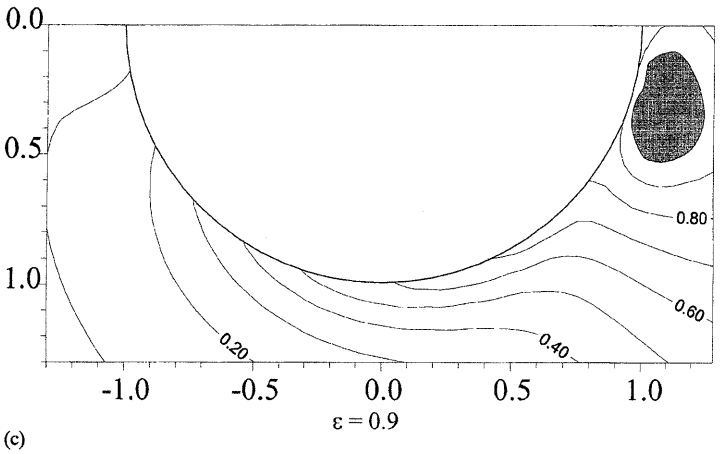

Fig. 5 The region stressed at 90 per cent or more of the maximum von Mises parameter ($\nu = 0.3$)

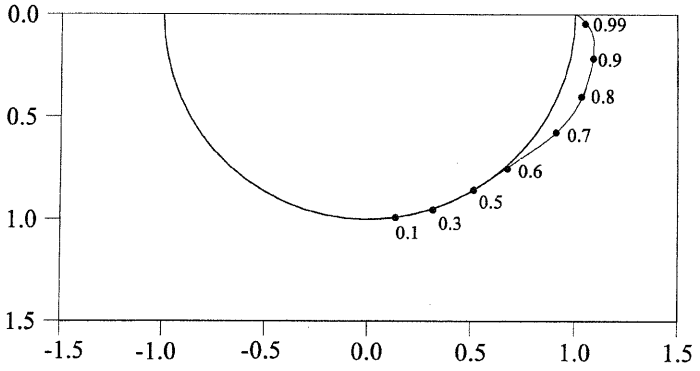

Fig. 6 The points of first yield for different eccentricity ratios ε

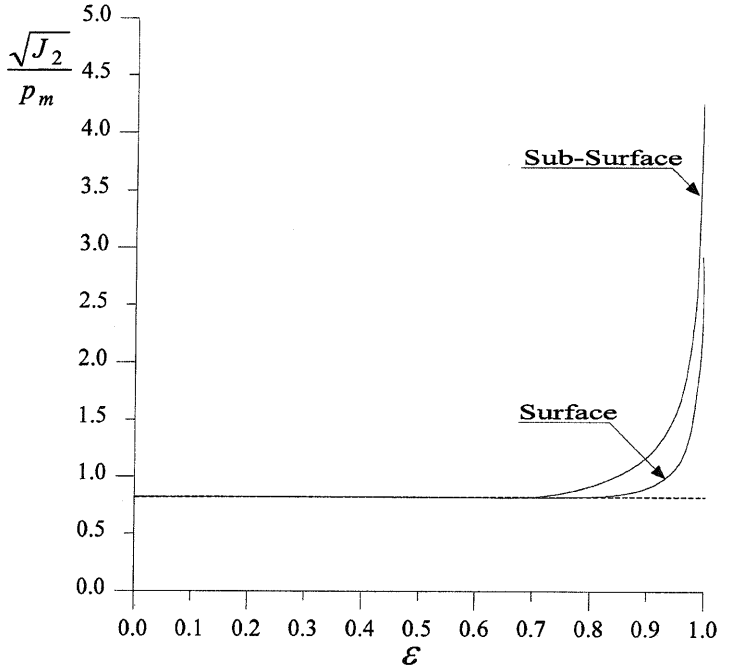

Fig. 7 The subsurface and surface maxima of the von Mises parameter against the eccentricity ratio ε

working under more severe conditions, and for these cases a more refined procedure is needed. Equation (1) gives the working pressure $p_m = W/(2R)$, and invoking the von Mises criterion, the maximum allowable specific pressure to avoid yielding is

$$p_m = \frac{k}{[(\sqrt{J_2})/p_m]_{max}} \tag{11}$$

as at yield $\sqrt{J_2} = k$, where k is the yield stress of the material in pure shear.

As an example, in Fig. 8, the working specific pressure and the maximum allowable specific pressure are illustrated, as solid and dashed curves respectively, against the eccentricity ratio ε. The curves are referred to the absolute viscosity $\mu = 0.01$ of the lubricant and a relative radial clearance $\psi = 10^{-3}$, common values in similar applications. The working specific pressure is plotted for three different journal speeds, while the maximum allowable pressure is made to vary with respect to the yield stress in pure shear $\sigma_y[\sigma_y = (\sqrt{3})k]$. Observing Fig. 8, it is noted that the curves of the working and the maximum allowable specific pressure cross each other, say, at $\varepsilon = \varepsilon_c$. If $\varepsilon_c \leqslant 0.7$, yielding is avoided as stated before, i.e. by setting

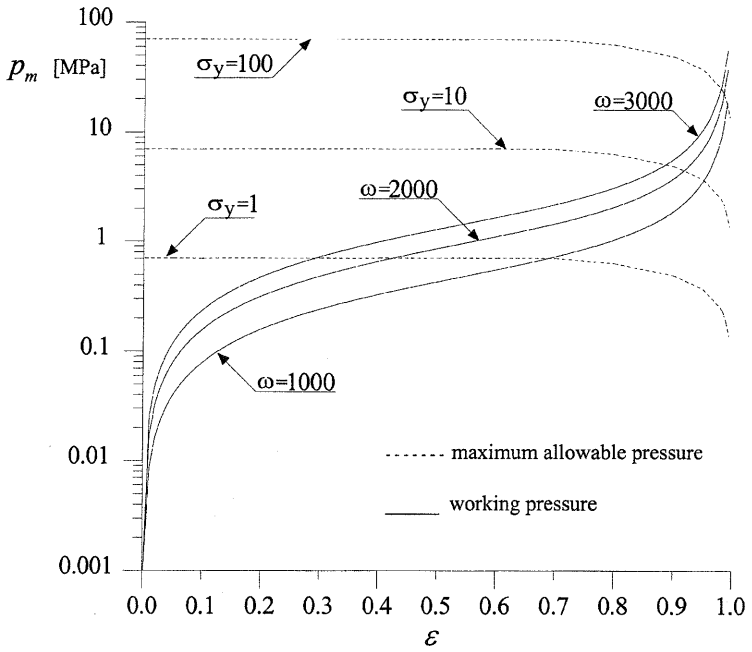

Fig. 8 The working and the maximum allowable specific pressures against the eccentricity ratio ε ($\mu = 0.01$ and $\psi = 10^{-3}$)

$p_m \leqslant 1.22k$, while for larger eccentricity ratios the actual intersection gives the maximum operating eccentricity ratio.

4 CONCLUSIONS

As intuitively expected, the tendency to yield increases with increasing magnitude of the applied load. Moreover, to guarantee the avoidance of yielding, bearings should work with eccentricity ratios smaller than 0.7, together with a specific pressure smaller than $1.22k$, where k is the yield stress of the material in pure shear. If this is considered too conservative, and it is necessary to operate with larger eccentricity ratios, the maximum eccentricity ratio is given by yielding of the material according to the charts given in the paper.

ACKNOWLEDGEMENT

Michele Ciavarella is pleased to acknowledge the support from Consiglio Nazionale delle Ricerche (Borsa per l'estero 203.07.26 del 12.09.96), for his visit to the University of Oxford, where the present work was started.

REFERENCES

1 **Hills, D. A.** and **Sackfield, A.** An analysis of the required strength of journal bearing materials. In *Developments in Numerical and Experimental Methods Applied to Tribology*, Proceedings of the Tenth Leeds–Lyon Symposium on *Tribology*, Lyon, September 1983, 1984 pp. 55–60 (Butterworth, London).

2 **Hacifazlioglu, S.** and **Karadeniz, S.** A parametric study of stress sources in journal bearings. *Int. J. Mech. Sci.*, 1996, **38**, 1001–1015.

3 **Singh, S.** Stresses and deformation of a long hydrodynamic journal bearing. *Computer Structs*, 1993, **48**, 81–86.

4 **Cameron, A.** *The Principles of Lubrication*, 1966 (Longmans, London).

5 **Green, A. E.** and **Zerna, W.** *Theoretical Elasticity*, 1954 (Clarendon, Oxford).

6 **Davis, F. P.** and **Rabinowitz, P.** *Methods of Numerical Integration*, 2nd edition, 1984 (Academic Press, New York).

7 **Hills, D. A., Nowell, D.** and **Sackfield, A.** *Mechanics of Elastic Contacts*, 1993 (Butterworth–Heinemann, Oxford).

APPENDIX 1

Starting from the full-Sommerfeld pressure distribution (see Section 12.7 of reference [**4**])

$$p(\theta, \varepsilon) = \frac{6\mu\omega}{\psi^2} \frac{\varepsilon}{2+\varepsilon^2} \frac{\sin\theta\,(2+\varepsilon\cos\theta)}{(1+\varepsilon\cos\theta)^2}, \qquad \theta \in [0, 2\pi] \tag{12}$$

For the half-Sommerfeld distribution, equation (12) holds only on the active arc of the bearing while, on the inactive arc of the bearing (i.e. $\theta \in [\pi, 2\pi]$), the pressure is null.

The applied load W and the attitude angle β may be evaluated by employing the load components

$$W_x = \int_0^{\pi} p \cos\theta \, R_s \, d\theta, \qquad W_y = \int_0^{\pi} p \sin\theta \, R_s \, d\theta \quad (13)$$

as

$$W = \sqrt{(W_x^2 + W_y^2)}, \qquad \tan\beta = \frac{W_y}{W_x} \quad (14)$$

Using the Sommerfeld substitution (see Section 12.5 of reference [4]),

$$\cos\gamma = \frac{\epsilon + \cos\theta}{1 + \epsilon\cos\theta}$$

gives

$$\cos\theta = \frac{\cos\gamma - \varepsilon}{1 - \varepsilon\cos\gamma}, \qquad \sin\theta = \frac{\sin\gamma}{1 - \varepsilon\cos\gamma}\sqrt{(1 - \varepsilon^2)} \quad (15)$$

Solving the elementary integrals, after a little algebra, it follows that

$$W_x = C\int_0^{\pi} \frac{\sin\theta\,(2 + \varepsilon\cos\theta)}{(1 + \varepsilon\cos\theta)^2}\cos\theta \, d\theta = C\frac{2\varepsilon}{1 - \varepsilon^2} \quad (16)$$

and

$$W_y = C\int_0^{\pi} \frac{\sin^2\theta\,(2 + \varepsilon\cos\theta)}{(1 + \varepsilon\cos\theta)^2} d\theta = C\frac{\pi}{\sqrt{(1 - \varepsilon^2)}} \quad (17)$$

where we have indicated as C the constant

$$C = \frac{6\mu\omega}{\psi^2}\frac{\varepsilon}{2 + \varepsilon^2}R_s \quad (18)$$

obtaining finally equations (2) and (3).

APPENDIX 2

The stress influence functions are obtained after a little algebra as

$$g_{rr} = \frac{\rho^2 - 1}{2\rho^3}\left\{2\kappa_1\cos(\varphi - \theta) + \rho\frac{1 - 2\rho\cos(\varphi - \theta)}{\rho^2 - 2\rho\cos(\varphi - \theta) + 1} - \rho^2\frac{(\rho^2 + 1)\cos(\varphi - \theta) - 2\rho}{[\rho^2 - 2\rho\cos(\varphi - \theta) + 1]^2}\right\} \quad (19)$$

$$g_{\varphi\varphi} = \frac{1}{2\rho^3}\left\{2(\rho^2 + 1)\kappa_1\cos(\varphi - \theta) - \rho\frac{2\rho(\rho^2 + 1)\cos(\varphi - \theta) - 3(\rho^2 + 1) + 2}{\rho^2 - 2\rho\cos(\varphi - \theta) + 1} + \rho^2(\rho^2 - 1)\frac{(\rho^2 + 1)\cos(\varphi - \theta) - 2\rho}{[\rho^2 - 2\rho\cos(\varphi - \theta) + 1]^2}\right\} \quad (20)$$

$$g_{r\varphi} = \frac{\rho^2 - 1}{2\rho^3}\left\{2\kappa_1 - \frac{(\rho^2 - 1)\rho^2}{[\rho^2 - 2\rho\cos(\varphi - \theta) + 1]^2}\right\} \times \sin(\varphi - \theta) \quad (21)$$

where $\kappa_1 = \kappa/(\kappa + 1)$.